Surface Tension and Compression Modulus Anisotropies of a Phospholipid Monolayer Spread on Water and on Formamide

Arnaud Saint-Jalmes, Michel Assenheimer,† and François Gallet*,‡

Laboratoire de Physique Statistique de l'Ecole Normale Supérieure (U.R.A. 1306 Associée au C.N.R.S. et aux Universités Paris 6 et Paris 7), 24 Rue Lhomond, 75231 Paris Cedex 05, France

Received: December 16, 1997; In Final Form: May 8, 1998

The elastic properties of the low-temperature solid phase of a 1,2-distearoyl-*sn*-glycero-3-phophatidylcholine (DSPC) monolayer spread at the air−water and at the air−formamide interfaces are studied by propagating surface waves in two perpendicular directions. On formamide, we detect anisotropies of both the surface tension and of the DSPC film compression modulus above a surface pressure threshold $\pi_c \approx 7$ mN/m, corresponding to the onset of a buckling instability of the solid film. Above the threshold, the 2D Poisson coefficient continuously decreases from 1 to 0.7, and the film is more compressible in the buckled direction than in the orthogonal one. For the same film on water, where no buckling occurs, no anisotropies are detected. This method also provides a reasonable value for the film surface viscosity.

1. Introduction

To investigate the effective role of the liquid subphase on Langmuir film properties, recent studies[1,2] have compared the properties of a 1,2-distearoyl-*sn*-glycero-3-phophatidylcholine (DSPC) film spread on water and on formamide. Indeed, among other liquids, formamide (CHO−NH_2, surface tension $\gamma_0 = 58.2$ mN/m at 20 °C) can be used as an alternative nonaqueous polar solvent to support amphiphilic monolayers.[3]

The phase diagram of DSPC on formamide has recently been determined from surface isotherms, fluorescence microscopy observations,[1] and X-ray diffraction.[2] The same techniques were previously used to investigate the phase diagram on water.[4−5] In both these systems the main transition from the fluid phase (gaseous or liquid phase) to the condensed phase is first-order. However, there are important differences between the condensed solid phases spread on formamide and those on water, as will be shown below.

On formamide, besides a mesophase localized in a small region of the phase diagram (20 °C < T < 25 °C, 0 < π < 3 mN/m), there is one single solid crystalline phase above the main fluid/condensed transition line. The structure of this solid phase has been determined by grazing incidence X-ray diffraction.[2] It does not change in the investigated pressure range (0 < π < 50 mN/m) and temperature range (10 °C < T < 25 °C). The chains are organized on an oblique lattice, and their tilt angle measured from Bragg rod scans is $\theta = 35°$. The area per molecule is $A = 46$ Å^2, a result consistent with the packing of two tilted chains. From the slight displacement of the diffraction peaks with increasing surface pressure, one can infer the molecular compression modulus $\epsilon = -A\, d\pi/dA = 3500$ mN/m, indicating that the phase is very stiff.

As on formamide, a solid crystalline phase exists on water. The chains are organized on a rectangular lattice, but the structure changes with pressure; the tilt angle decreases as the pressure increases. At high pressure, the area A per molecule is 41 Å^2, which confirms that the chains are less tilted on water than on formamide. Some authors reported the existence of a tilted−untilted transition at high surface pressure,[4] although this was not confirmed by X-ray diffraction studies. In this solid phase, one measures a compression modulus $\epsilon = -A\, d\pi/dA = 350$ mN/m, much smaller than on formamide.

Changing the subphase does not only induce differences in the phase diagram; in the crystalline phase spread on formamide, a buckling instability develops above a surface pressure threshold π_c. This instability generates a stable, permanent, and roughly periodic vertical deformation of the interface, which does not occur in the solid phase on water. It was first observed with a regular optical microscope,[6] but a complete quantitative characterization was made by studying light scattering from the buckled interface;[7] a nonzero scattered intensity is detected above the surface pressure threshold $\pi_c \approx 7$mN/m. The buckling amplitude varies from zero at the threshold to a few nanometers at $\pi \approx 30$ mN/m, and the typical length scale of the deformation is $\lambda \approx 16$ μm. Brewster angle microscopy observations also provide information on this instability and on the texture of the crystalline phase; below the threshold, the layer is organized in domains corresponding to a fixed in-plane tilt direction. The typical domain size is 7 μm, comparable to the characteristic buckling length scale.

The large compression modulus ϵ of the solid phase on formamide and the tilt angle texture are important parameters in a theoretical description of the instability. Recently, we have proposed a model based on the coupling between the film elasticity and the variations of the tilt orientation. The predictions are in good agreement with experimental data.[7] In particular, we found that the instability wavelength should be twice the domain size, which is consistent with our observations.

Since the elastic properties of the layer are relevant, a question arises about a possible stress anisotropy in the film. Indeed, it is well-known that in dense phases the surface pressure π may no longer be isotropic[8] and should be replaced by a two-dimensional surface stress tensor $\pi_{ij} = \gamma_0 - \gamma_{ij}$. The compo-

* To whom correspondence should be addressed.
† Present address: CI Systems, P.O. Box 147, 10551 Migdal Ha'Emek, Israel.
‡ Present address: LBHP, Case 7056, 2 Place Jussieu, 75251 Paris Cedex 05, France.

S1089-5647(98)00541-0 CCC: $15.00
Published on Web 07/03/1998

nents of this tensor can be measured by using the surface wave dispersion relation. The method consists of exciting a surface wave and measuring its wavevector and attenuation, from which one infers the surface tension γ_{ii} and compression modulus ϵ_{ii} in the direction of propagation. We built a surface wave excitation setup in order to look for a possible anisotropy in DSPC films, both on water and on formamide substrates. In this last case we were also interested in the correlation between the anisotropy and the buckling instability.

In this paper, we first present the dispersion relation for a surface wave propagating on a viscous liquid covered by a monolayer. Then we derive an explicit relation to infer the surface stress and the compression modulus from the complex wavenumber. After describing the experimental setup, we show some calibration data obtained on a pure liquid and on a liquid covered by a fluid film. We carefully discuss the influence of various parameters to get the best accuracy. Then we present the results for the crystalline phases of DSPC on water and on formamide. On water, the mechanical properties of DSPC films always remain isotropic. In contrast, on formamide we detect some anisotropy of both surface stresses and compression moduli in DSPC films above a pressure threshold π_0, closely related to the buckling instability threshold of the interface.

2. Surface Wave Method

2.1. Principle and Dispersion Relation. The well-known dispersion relation $\omega(k)$ of surface waves propagating on a nonviscous liquid of infinite depth was first derived by Lord Kelvin[9]:

$$\rho\omega^2 = \gamma k^3 + \rho g k \tag{1}$$

In this formula ρ is the liquid density, g the gravity acceleration, $f = \omega/(2\pi)$ the frequency, and k the wave vector modulus. For a viscous fluid, the wave vector becomes complex and its imaginary part represents the wave damping. When a film is spread at the interface, the subphase viscosity couples the surface waves in the liquid and the compression waves in the film. The periodic motion of liquid particles at the interface induces a synchronous compression wave in the film. The film response is governed by its elasticity, which determines surface tension gradients. Then the compression modulus $\epsilon = -A\,\mathrm{d}\pi/\mathrm{d}A$ should appear in the modified dispersion relation. According to refs 8 and 10, this relation can be written as

$$[\gamma k^3 + \rho g k - \rho\omega^2 - \mathrm{i}\omega\eta k(k+m)][\epsilon k^3 - \mathrm{i}\omega\eta k(k+m)] = [\mathrm{i}\omega\eta k(k-m)]^2 \tag{2}$$

where $k = k_r + \mathrm{i}k_i$ is the complex wave vector amplitude, k_i the wave damping coefficient, η the subphase viscosity, and m is defined by

$$m^2 = k^2 - \frac{\mathrm{i}\omega\rho}{\eta}$$

the real part of m being positive. From eq 2, the unknown quantities γ and ϵ are in principle completely determined by the measurements of k_i and k_r. However, eq 2 is not written in a suitable form to directly infer γ and ϵ. In the appendix, we derive explicit expressions (eqs A2 and A3) for γ and ϵ as a function of k_r and k_i.

This approach leads to two sets of solutions: (γ^+, ϵ^+) and (γ^-, ϵ^-). Numerical simulations shed light on these solutions and on their respective domain of application. We found that the first one (+) corresponds to low ϵ phases (liquidlike phases or coexistence plateau) and the second one (−) to high ϵ (condensed phase). When a soft phase is compressed to a rigid one, the two sets of solutions join at a given point, where one shifts from one solution to the other in order to preserve the continuity for the surface tension and the compression modulus. These simulations have also shown that, although the dispersion relation couples the surface tension and the compression modulus, γ remains mainly dependent on k_r and ϵ on k_i.

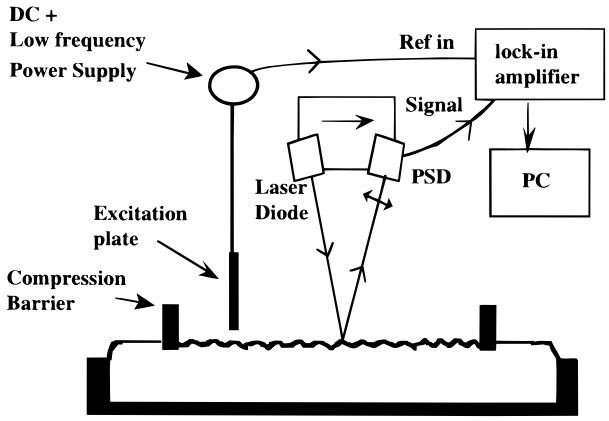

Figure 1. Scheme of the experimental setup used to excite and detect surface waves. The full setup can rotate around a vertical axis to probe the surface in any in-plane direction.

We supposed up to now that γ and ϵ are real quantities. In physical cases, surface tension γ and compression modulus ϵ may have a small imaginary part: ϵ_i is directly proportional to the surface viscosity η_s through the relation $\epsilon_i = -2\eta_s\omega$.[11] The imaginary part of the surface tension γ_i is therefore related to ϵ_i through the projection on the imaginary axis of the equation $\epsilon = A\,\mathrm{d}\gamma/\mathrm{d}A$. In this case, the expressions for γ and ϵ given in the appendix remain valid, provided that one replaces A_i by $A_i - \gamma_i$ and B_i by $B_i - \epsilon_i$.

Finally, numerical simulations have shown some other nonlinear behaviors of the dispersion relation. One of them concerns the accuracy of the experimental determination of ϵ; in a rigid dense phase with a large compressibility modulus ($\epsilon > 50$ mN/m), we noticed that a small variation of k_i makes ϵ vary in a wide range. We give below an example where a 0.2% variation for k_i corresponds to a 1.5% variation for ϵ. Thus, the measurement of k_i must be very accurate to get a correct value of ϵ.

2.2. Experimental Setup. Our homemade Langmuir trough has been described elsewhere.[6] It is enclosed in a glovebox and is thermally regulated by an external water circulation. It is built with a double barrier to allow symmetrical compression around the observation area. The surface pressure is currently controlled with a Wilhelmy balance (Riegler and Kierstein). The setup for the excitation and detection of surface waves (Figure 1) is similar to the one described in ref 8. A horizontal copper plate (6 cm long) is driven by a dc voltage (100−300 V) superimposed on an ac voltage (amplitude of 50−150 V) at frequency ω. This plate excites a surface wave, which is a plane wave in its vicinity. A laser beam is reflected by the surface toward a position sensitive detector (PSD), delivering a signal proportional to the surface vertical displacement. The laser diode and the sensor are mounted on a motorized translation plate. The PSD signal is sent to a lock-in amplifier, which measures the amplitude and the phase of the propagating wave as a function of the distance from the excitation plate. Usual excitation frequencies are in the range 100−500 Hz for a typical 2 mm wavelength and 1 cm damping length on formamide. The

full excitation and detection setup may rotate around a vertical axis in order to generate a wave propagating in any in-plane direction. In the following, we restrict the study to waves propagating along the compression direction (Ox direction), or perpendicular to it (Oy direction). In this coordinate system, and because of the symmetry of the compression trough, we expect that the stress tensor remains diagonal and that γ_{xy} is zero.

3. Results

Before presenting original results concerning solid DSPC films on water and on formamide (sections 3.2 and 3.3), we show that the method leads to accurate measurements, provided that one includes in the analysis extra parameters such as air viscosity, or temperature and viscosity variations of the liquid.

3.1. Calibration and Tests. *3.1.1. Free Liquid Surface*. We checked that for an interface without film, we measure the free liquid surface tension γ_0 and the compression modulus $\epsilon = 0$. Practically, we measure k_r and k_i for a wave propagating on a free liquid surface at regulated temperature, we calculate γ and ϵ according to formulas A2 and A3 given in the appendix using the tabulated value of the liquid viscosity η for water and formamide.[12] Actually, if we do not take into account the viscosity η' of the above fluid (air), we do not exactly find $\gamma = \gamma_0$ and $\epsilon = 0$. For instance, for pure water at 20 °C, taking $\eta = 1.0$ mPa s and $\eta' = 0$, we get $\gamma = 71.9 \pm 0.1$ mN/m and $\epsilon = 1.0 \pm 0.1$ mN/m instead of the expected $\gamma_0 = 72.75$ mN/m and $\epsilon = 0$ mN/m. To get the correct values, we need to modify the dispersion relation in order to account for the air viscosity η' ($\eta' = 0.018$ mPa s at $T = 20$ °C) in the following way:

$$(\gamma k^3 + (\rho - \rho')gk - (\rho + \rho')\omega^2 - i\omega k(\eta(k+m) - \eta'(k+m')))(\epsilon k^3 - i\omega k(\eta(k+m) - \eta'(k+m'))) = (i\omega k(\eta(m-k) - \eta'(m'-k))^2 \quad (3)$$

where ρ' is the air density and $m'^2 = k^2 - i\omega\rho'/\eta'$. There is no difficulty in including these modifications in the dispersion relation analysis presented in the appendix.

Within this new formulation, the accuracy of the determination of the surface tension is good enough to use our setup as a viscometer for the liquid or as a thermometer for the interface. For instance, we have excited waves on the free surface of liquid formamide thermostated at bulk temperature T_b, while keeping the air temperature T_a constant at 20 °C. We adjust the viscosity η to get $\epsilon = 0$ (no film) and compare η to the values tabulated versus temperature.[12] As long as T_b is not too different from T_a, the interface temperature T_i deduced from the viscosity determination is equal to T_b: for instance, if $T_b = 18$ °C, $T_i = 18$ °C. For lower T_b, we get $T_b < T_i < T_a$; for instance, we measured $T_b = 8.4$ °C and $T_i = 10.3$ °C. The vertical thermal gradient increases when cooling the bulk. In principle, changing the frequency, and thus the penetration depth of the surface wave, could be a method to map the vertical temperature gradient. However, it is hard to extrapolate this method to a film-covered liquid surface because the monolayer probably affects the gradient shape.

Another use of this setup as a viscometer is directly related to the high hydrophilic character of formamide. As described above, we measure the viscosity of pure formamide with no film ($\epsilon = 0$) as a function of time, over a few days. We find that the viscosity decreases with time (from 4.6 to 3.5 mPa s over 60 h) because formamide absorbs the residual water vapor contained in the glovebox volume. Once the glovebox is filled with dry nitrogen gas, the formamide viscosity remains constant ($\Delta\eta$ was only 0.1 mPa s over 24 h). In the following section concerning film-covered interfaces, special care was devoted to always make measurements in a dry atmosphere.

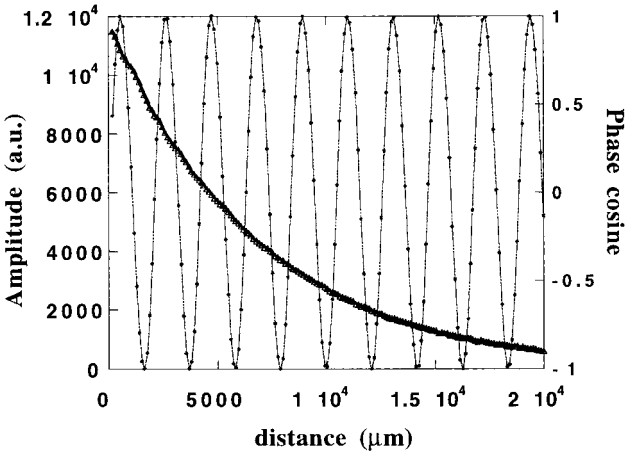

Figure 2. Typical recording of the surface wave phase and amplitude as a function of increasing distance from the source. A DSPC film is deposited on water at $T_i = 12$ °C. The wave frequency is 323 Hz. The best fits are also shown; the agreement with the expected sinusoidal and exponential variations is excellent. The measured values for the real and the imaginary parts of the wave vector are $k_r = 4254.42 \pm 0.01$ m^{-1} and $k_i = 123.8 \pm 0.3$ m^{-1}.

3.1.2. Fluid Monolayer with a First-Order Transition. As shown below, we also verified that the surface wave probe provides the same results as the Wilhelmy plate technique in the standard case of a fluid monolayer. We checked the validity of our data analysis, in particular the transition region between the two sets of solutions (γ^+, ϵ^+) and (γ^-, ϵ^-).

The isotherm of 1,2-dipalmitoyl-*sn*-glycero-3-phophatidylcholine (DPPC) on formamide at 21.5 °C presents a pressure increase from 0 to 9 mN/m corresponding to the pure liquid phase, followed by a first-order transition plateau between this phase and a condensed one. We obtained the same isotherm by the Wilhelmy plate and the wave propagation method and found as expected that the (+) solution is the physical one in the low-compression modulus region (typically for $\epsilon < 0.2\ \gamma$), which corresponds to the very low-pressure region and to the transition plateau. In contrast, the (−) solution must be kept in the pure liquid phase and in the pure condensed phase, roughly when $\epsilon > 0.2\gamma$. There are two points on the isotherm (on both sides of the plateau) where the two sets of solutions smoothly connect.

3.2. DSPC on Water. The isotherm of DSPC on water at 12 °C presents a very low-pressure plateau ($\pi < 0.2$ mN/m) followed by a rapid pressure increase corresponding to the solid phase. After each compression step in the solid phase, we let the film relax toward equilibrium and measure both surface stresses $\pi_{xx} = \gamma_0 - \gamma_{xx}$ and $\pi_{yy} = \gamma_0 - \gamma_{yy}$ in x and y directions. Simultaneously, we measure the surface pressure π_w with the Wilhelmy balance. The temperature is regulated so that $T_i = 12$ °C, and the x axis is parallel to the compression direction.

A typical recording of the surface wave phase and amplitude as a function of increasing distance from the source is presented in Figure 2. The wave propagates in the x direction at frequency $f = 323$ Hz. The best fits are also shown; the agreement with the expected sinusoidal and exponential variations is excellent. From this recording we measure the real and imaginary parts of the wave vector: $k_r = 4254.42 \pm 0.01$ m^{-1} and $k_i = 123.8 \pm 0.3$ m^{-1}. Surface stress and compression modulus are calculated with formulas A2 and A3 after averaging over several successive runs. For this example we find $\gamma_{xx} = 53.1 \pm 0.1$

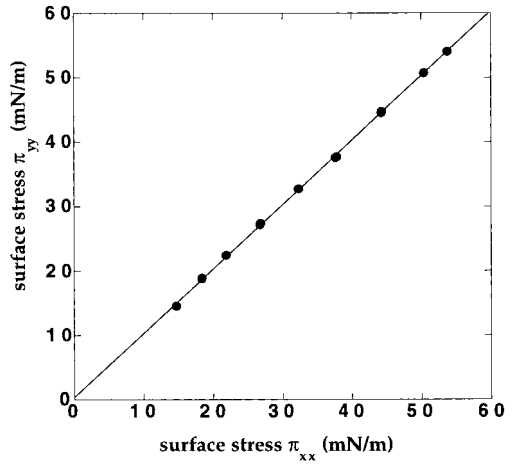

Figure 3. Surface stress π_{yy} vs π_{xx} for a DSPC film spread on water at $T_i = 12$ °C. Within experimental error, $\pi_{yy} = \pi_{xx}$ and no surface stress anisotropy is detected.

mN/m ($\pi_{xx} = 20.4$ mN/m) and $\epsilon_{xx} = 130 \pm 2$ mN/m. The typical accuracy on the determination of γ is 0.1 mN/m. It is usually not as good for ϵ because of the structure of the dispersion relation; in rigid phases, a small k_i variation leads to a large variation of ϵ. The precise knowledge of the viscosity η is also important for the accurate determination of ϵ.

Upon a pressure increase, we do not detect any surface stress anisotropy for the solid phase of a DSPC film spread on water. We measure $\pi = \pi_{xx} = \pi_{yy}$ up to the film collapse (Figure 3). On the other hand, we find most of the time that π_w is smaller than π. This confirms that the Wilhelmy plate is not a reliable method for measuring the surface pressure in dense phases.

Similarly, no wave-damping anisotropy has been detected. As for the surface tension, the compression moduli along both directions x and y are equal. Their typical value varies from 50 to 150 mN/m with increasing pressure.

3.3. DSPC on Formamide. Similar experiments have been performed on formamide. We built the isotherms by reporting the measured values $\boldsymbol{\pi}_{xx}$, $\boldsymbol{\pi}_{yy}$, and $\boldsymbol{\pi}_w$ as a function of the area per molecule. After each compression step ($\Delta A \approx 1$ Å^2), we wait until the surface pressure stabilizes. This takes about half an hour, which is the estimated time for the system to relax toward equilibrium. Figure 4 shows the results of two experiments at $T_i = 14$ °C. Below $\boldsymbol{\pi}_0 \approx 5$mN/m, we note that $\boldsymbol{\pi}_{xx} = \boldsymbol{\pi}_{yy} \approx \boldsymbol{\pi}_w$; there is no in-plane anisotropy and no clear difference between surface wave and Wilhelmy balance data. Above $\boldsymbol{\pi}_0$, some anisotropy appears and $\boldsymbol{\pi}_{xx}$ is always larger than $\boldsymbol{\pi}_{yy}$. In our geometry, there is no strain along the fixed borders of the trough, and the 2D Poisson coefficient $\boldsymbol{\sigma}_{||}$ ($0 < \boldsymbol{\sigma}_{||} < 1$ [13]) is defined by $\boldsymbol{\sigma}_{||} = \boldsymbol{\pi}_{yy}/\boldsymbol{\pi}_{xx}$. We measure a monotonic decrease of $\boldsymbol{\sigma}_{||}$ from 1 at $\boldsymbol{\pi}_0$ to 0.7 at $\boldsymbol{\pi}_{xx} = 35$ mN/m. In this pressure range, the Wilhelmy balance data are not reproducible from one experiment to the other. In Figure 4, we have $\pi_w < \pi_{yy} < \pi_{xx}$, but in Figure 5 $\pi_{yy} < \pi_w < \pi_{xx}$. On the average, it seems that π_w is the more often closer to π_{yy} than to π_{xx}, as can be expected.[6]

Upon decompression from a highly compressed layer, we observe that the anisotropy is inverted after each decompression step: $\pi_{yy} > \pi_{xx}$ (Figure 5). Further decompressing below π_0, one recovers the isotropic result $\pi_{xx} = \pi_{yy} = \pi_w$. The anisotropy threshold π_0 was precisely determined by averaging over several runs. We found $\langle\pi_0\rangle = 6 \pm 1$ mN/m.

We also noticed that the out-of-equilibrium stress anisotropy is a maximum immediately after a compression step and then decreases toward a final nonzero equilibrium value. We think

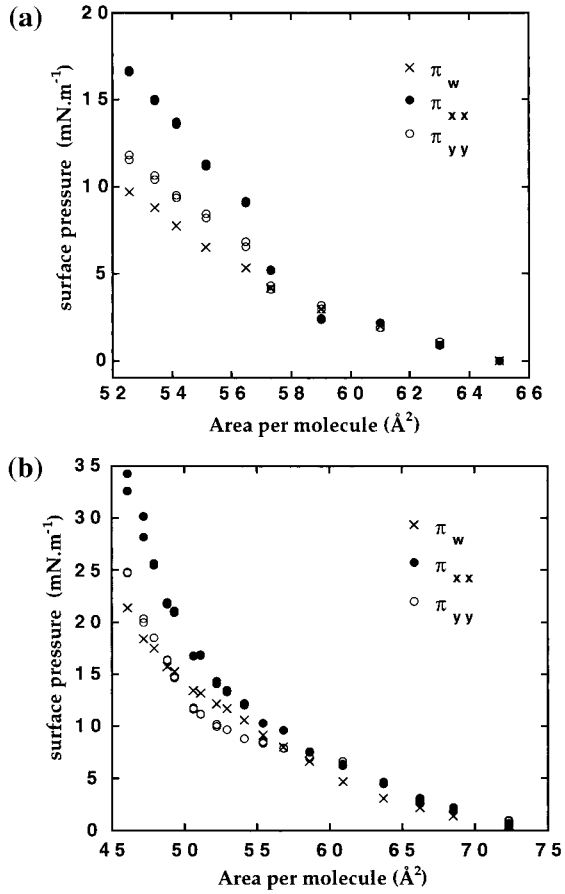

Figure 4. Surface isotherms for DSPC on formamide at $T_i = 14$ °C from two different experiments. The surface stresses π_{xx} and π_{yy} are determined from the surface wave dispersion relation (eq 2), and π_w is measured with a Wilhelmy plate. We observe that $\pi_{xx} = \pi_{yy} = \pi_w$ up to a threshold $\pi_0 \approx 5$ mN/m. Above π_0 some anisotropy appears and $\pi_{xx} > \pi_{yy}$. Note that $\pi_w < \pi_{yy} < \pi_{xx}$ in part a while $\pi_{yy} < \pi_w < \pi_{xx}$ in part b, which demonstrates that the Wilhelmy plate method is not reliable.

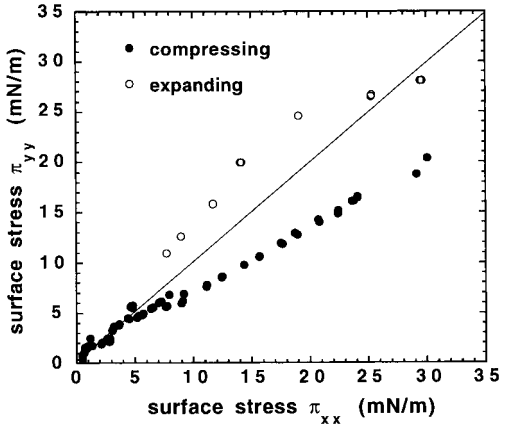

Figure 5. Plot of π_{yy} vs π_{xx} during a compression−expansion cycle (DSPC on formamide at $T_i = 14$ °C). Below the threshold $\pi_0 \approx 5$ mN/m, the film is isotropic. The surface stress anisotropy is inverted between compression and expansion, but the film behavior is reversible.

that, before reaching equilibrium, some plastic deformations are responsible for relaxing part of the stresses.

In Figure 6 we plotted the inverse $1/\epsilon_{xx}$ and $1/\epsilon_{yy}$ of the compression modulus versus surface stresses π_{xx} and π_{yy} from a representative experiment. Clear anisotropy also appears between x and y directions above a threshold $\pi_1 = 7$mN/m. This mainly reflects the anisotropy of the wave-damping

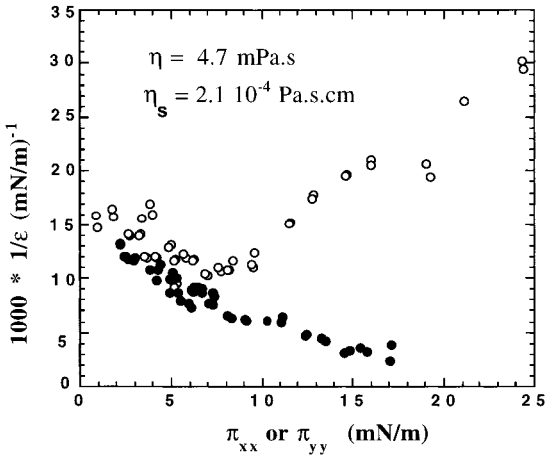

Figure 6. Plot of $1/\epsilon_{xx}$ vs π_{xx} (○) and $1/\epsilon_{yy}$ vs π_{yy} (●) for DSPC on formamide at $T_i = 14$ °C. ϵ_{xx} and ϵ_{yy} are the monolayer compression moduli calculated from the dispersion relation (eq 2). The bulk formamide viscosity is η ($T = 14$ °C) = 4.7 mPa s, and the film surface viscosity is adjusted to $\eta_s = 2.1 \times 10^{-4}$ Pa s cm. Below $\pi_1 = 7$mN/m, $\epsilon_{xx} = \epsilon_{yy}$. Above π_1, which we identify as the buckling threshold, ϵ_{xx} starts decreasing while ϵ_{yy} keeps increasing with pressure.

coefficient k_i. For $\pi < \pi_1$, ϵ_{xx} and ϵ_{yy} are approximately equal and both increase with pressure. Their common values roughly correspond to the one calculated from the isotherm. At π_1, ϵ_{xx} reaches a maximum and then decreases with increasing π_{xx}. The behavior of ϵ_{yy} is different, since it keeps increasing in the whole range of surface pressure. Averaging over several experiments, we found $\pi_1 = 7 \pm 1$ mN/m.

To extract ϵ from a set of measurements (k_i, k_r), we had to consider a negative imaginary part ϵ_i for ϵ, corresponding to a positive surface viscosity $\eta_s = -\epsilon_i/(2\omega)$. The formamide viscosity η is constant in dry atmosphere, and we took the tabulated value at $T_i = 14$ °C, $\eta = 4.7$ mPa s. If both ϵ_{xx} and ϵ_{yy} were calculated with $\eta_s = 0$, some of the obtained values would be negative, which is unphysical. Adding a small $\eta_s > 0$ only vertically translates the curves $1/\epsilon_{xx}$ and $1/\epsilon_{yy}$ versus π and does not affect their general behavior. The choice of η_s was made to get positive ϵ values and to have $1/\epsilon_{yy}$ close to 0 at high pressure. This leads to an estimate of surface viscosity. In Figure 6, we used $\eta_s = 2.1 \times 10^{-4}$ Pa s cm. By the channel flow method,[14,15] surface viscosities were found in the range $(1-20) \times 10^{-5}$ Pa s cm. Our estimate is reasonable, although somewhat large, which is probably related to the stiffness of the monolayer. In all cases the imaginary part ϵ_i of ϵ remains small compared with the real part ϵ_r, since $\epsilon_r/\epsilon_i \approx 100$.

4. Discussion: Comparison of Water/Formamide and Relation to Buckling

The main result of this study lies in the different behavior for surface stresses and compression moduli of the solid DSPC phase, depending on the nature of the subphase. On water, no anisotropy is detected in the full pressure range. On formamide, compression modulus anisotropy is detected above $\pi_1 = 7 \pm 1$ mN/m. We think that the onset for the compression modulus anisotropy π_1 can be identified to be at the buckling threshold $\pi_c = 7 \pm 1$ mN/m. Indeed, we observed that the buckling deformation wave vector is preferentially parallel to the compression direction (x direction), as shown on optical microscope and Brewster angle microscope images. Then the respective behavior of ϵ_{xx} and ϵ_{yy} is easy to interpret; for example, for a corrugated plate, it is easier to compress the buckled monolayer in the x direction and more difficult in the perpendicular one. On the other hand, surface stress anisotropy develops above $\pi_0 = 6 \pm 1$ mN/m. Considering our accuracy, we cannot decide whether π_0 equals π_c or not, but it is reasonable to assume that both the surface stress anisotropy and the compression modulus anisotropy are strongly correlated to the buckling instability.

We also mentioned that the Wilhelmy plate method is not reliable in a dense phase. Even when the monolayer remains isotropic (as on water), there is a discrepancy between the pressure measured by surface wave excitation and by the Wilhelmy plate. When the surface stresses are anisotropic (as on formamide), the Wilhelmy plate is definitely not suitable. However, up to the threshold, the two methods give the same value for the isotropic surface pressure. Thus, the initial measurements of the buckling threshold with a Wilhelmy plate were correct.[7]

Our last remark concerns the comparison among the compression moduli obtained from the surface wave probe, those obtained by the usual isotherm method, and those calculated from X-ray diffraction data. The last method leads to much larger values than the two other ones (thousands versus hundreds of mN/m, respectively). This is due to a large difference in the typical observation scale. By X-ray diffraction, we measure the elastic response of a single crystallite, whose size is a few micrometers. By the two other methods, we average over a larger region of the monolayer, which includes several crystals, defects, boundaries, ... The average elastic response on a millimeter scale is probably dominated by these defects, which lower the compression modulus. Following the same kind of argument, we think that the surface stresses measured by the surface wave method on a millimeter scale are probably an average over a complex distribution of local stresses. In particular, these surface stresses could locally be high enough to lower the surface tension to zero, which would induce spontaneous buckling of the interface. This possible mechanism may explain the onset of buckling on formamide at a finite average surface tension $\gamma_c = 51$ mN/m.[16]

5. Conclusions

In this paper, we study the mechanical properties of a phospholipid crystalline monolayer both on water and on formamide by the surface wave excitation method. We write the dispersion relation under a form convenient for numerical treatment and data analysis. Experimental results show that this technique gives accurate measurements of the surface tension and of the monolayer compression modulus. For a free liquid surface, it can be used as a viscometer and also as a surface thermometer. For a formamide surface coated with a DSPC solid monolayer, there is clear evidence for surface stress anisotropy. In that case, the classical Wilhelmy plate method is no longer suitable. On formamide, we have also measured the compression modulus anisotropy, correlated to the buckling instability of the film. On water, no anisotropy is detected, which confirms that no buckling instability occurs in this case.

Acknowledgment. M.A. gratefully acknowledges support from a European Community fellowship (Human Capital and Mobility program).

Appendix

Starting from eq 2, we look for analytical expressions for γ and ϵ as functions of $k = k_r + ik_i$. We suppose that γ and ϵ are real quantities. We write the dispersion relation in the following way:

$$(A - \gamma)(B - \epsilon) = C \tag{A1}$$

A, B, and C are complex functions of k_r and k_i, defined as follows:

$$A = [\rho\omega^2/k - \rho g + i\omega\eta(k + m)]/k^2 = A_r + iA_i$$

$$B = [i\omega\eta(k + m)]/k^2 = B_r + iB_i$$

$$C = [i\omega\eta(k - m)]^2/k^4 = C_r + iC_i$$

with $m^2 = k^2 - i\omega\rho/\eta$.

To get explicit expressions of A_r , A_i, B_r , B_i, C_r, and C_i as functions of k_r and k_i, we introduce $\delta = m/k = \delta_r + i\delta_i$ and $\alpha = (\omega\rho/\eta)^{1/2}$.

One has

$$\delta_r = \left[\frac{1}{2}\left(1 - \frac{b^2}{a^2}\right)\left(1 + \sqrt{1 - \frac{c^2}{a^2 - b^2}}\right)\right]^{1/2}$$

and

$$\delta_i = -\frac{c^2}{2a^2\delta_r}$$

with the following definitions:

$$a = k_r^2 + k_i^2, \quad b^2 = 2\alpha^2 k_r k_i, \quad c^2 = \alpha^2(k_r^2 - k_i^2)$$

Then

$$A_r = \frac{k_r^3 - 3k_r k_i^2}{a^3} - \frac{g(k_r^2 - k_i^2)}{\omega^2 a^2} - \frac{\delta_i k_r - k_i(1 + \delta_r)}{a\alpha^2}$$

$$A_i = \frac{2gk_r k_i}{\omega^2 a^2} + \frac{k_i^3 - 3k_i k_r^2}{a^3} + \frac{\delta_i k_i + k_r(1 + \delta_r)}{a\alpha^2}$$

$$B_r = -\frac{\delta_i k_r - k_i(1 + \delta_r)}{a\alpha^2}$$

$$B_i = \frac{\delta_i k_i + k_r(1 + \delta_r)}{a\alpha^2}$$

$$C_r = \frac{-1}{a^2\alpha^4}((k_r(1 - \delta_r) - \delta_i k_i)^2 - (\delta_i k_r + k_i(1 - \delta_r))^2)$$

$$C_i = \frac{2}{a^2\alpha^4}(k_r(1 - \delta_r) - \delta_i k_i)(\delta_i k_r + k_i(1 - \delta_r))$$

Solving eq A1, one can finally write the two couples of solutions (γ^+, ϵ^+) and (γ^-, ϵ^-):

$$\epsilon_\pm = B_r - \frac{C_i}{2A_i} \pm \frac{\sqrt{C_i^2 - 4A_i B_i(A_i B_i + C_r)}}{2A_i} \tag{A2}$$

$$\gamma_\pm = A_r - \frac{C_i}{2B_i} \mp \frac{\sqrt{C_i^2 - 4A_i B_i(A_i B_i + C_r)}}{2B_i} \tag{A3}$$

References and Notes

(1) Graner, F.; Perez-Oyarzun, S.; Saint-Jalmes, A.; Flament, C.; Gallet, F. *J. Phys. II* **1995**, *5*, 313−322.

(2) Saint-Jalmes, A.; Graner, F.; Gallet, F.; Nassoy, P.; Goldmann, M. *Chem. Phys. Lett*. **1995**, *240*, 234.

(3) Weinbach, S. P.; Kjaer, K.; Als-Nielsen, J.; Lahav, M.; Leiserowitz, L. *J. Phys. Chem*. **1993**, *97*, 5200.

(4) Albrecht, O.; Gruler, H.; Sackmann, E. *J. Phys*. **1978**, *39*, 301.

(5) Kjaer, K.; Als-Nielsen, J.; Helm, C. A.; Laxhuber, L. A.; Möhwald, H. *Phys. Rev. Lett*. **1987**, *58*, 2224. Struth, B.; Scalas, E.; Brezesinski, G.; Möhwald, H.; Bringezu, F.; Bouwman, W. G.; Kjaer, K. *Nuovo Cimento* **1994**, *16* (9).

(6) Saint-Jalmes, A.; Graner, F.; Gallet, F.; Houchmandzadeh, B. *Europhys. Lett*. **1994**, *28*, 565.

(7) Saint-Jalmes, A.; Gallet, F. *Eur. Phys. J. B* **1998**, *2*, 489.

(8) Miyano, K. *Langmuir* **1990**, *6*, 1254−1259.

(9) Thomson, W. *Philos. Mag*. **1871**, *42*, 362.

(10) Bock, E. J. Adin Mann, J., Jr. *J. Colloid Interface Sci*. **1989**, *129*, 501.

(11) Earnshaw, J. C.; McGivern, R. C.; Winch, P. J. *J. Phys. (France)* **1988**, *49*, 1271.

(12) *Handbook of Chemistry and Physics*, 75th ed.; CRC Press: Boca Raton, FL, 1994; Section 6, p 241.

(13) Landau, L.; Lifchitz, E. *Theory of Elasticity*; Pergamon Press: Oxford, 1984.

(14) Sachetti, M.; Yu, H.; Zografi, G. *J. Chem. Phys*. 1993, 99 (1), 563.

(15) Relini, A.; Ciuchi, F.; Rolandi, R. *J. Phys. II* **1995**, *5*, 1209.

(16) Daillant, J. Private communication.